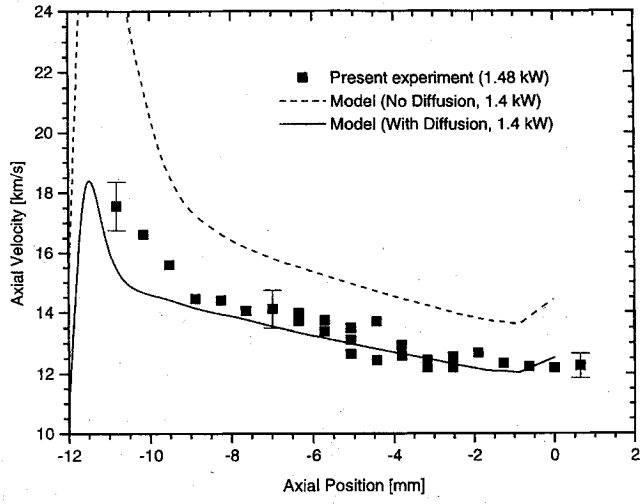

Fig. 2 Measured axial velocity along the arcjet centerline. Typical errors are shown. The measurements are compared to results of an arcjet model incorporating mass diffusion and without mass diffusion.

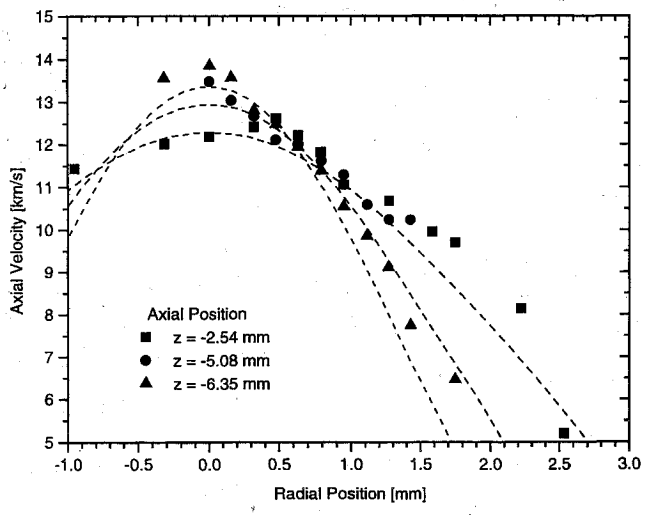

Fig. 3 Radial profiles of axial velocity at three axial locations within the arcjet nozzle. Errors are typically ±0.6 km/s. The dashed lines are results of the arcjet model (with diffusion) at the same axial locations as the measurements.

upstream from the exit plane). The LIF signal intensity dropped off quickly with radial position, indicating a rapid radial decrease in the $n = 2$ excited-state number density of atomic hydrogen. This loss in signal restricted the measurement domain to within approximately 2 mm of the nozzle centerline. The dashed lines in the figure are the model results at the same axial locations as the measurements. The measurements and the model show remarkably good agreement; however, the measured velocities are somewhat greater than those of the model away from the arcjet centerline. Although the centerline velocity decreases axially, the velocities away from the centerline increase with axially position. Because most of the mass convection occurs in this outer region, the total kinetic energy of the flow is clearly increasing downstream, as is expected in a supersonic diverging nozzle.

At present, experiments are under way to perform a more comprehensive study to map the velocity flowfield at various arcjet specific energies for both hydrogen and simulated hydrazine propellants.

Acknowledgments

This work was supported in part by the U.S. Air Force Office of Scientific Research and Olin Aerospace Company. Special acknowledgments are given to NASA Lewis Research Center for supplying the arcjet thruster and power supply and to G. W. Butler of Olin-Aerospace Company for providing the arcjet modeling results.

References

[1]Liebeskind, J. G., Hanson, R. K., and Cappelli, M. A., "Laser-Induced Fluorescence Diagnostic for Temperature and Velocity Measurements in a Hydrogen Arcjet Plume," *Journal of Applied Optics*, Vol. 32, No. 30, 1993, pp. 6117–6127.

[2]Liebeskind, J. G., Hanson, R. K., and Cappelli, M. A., "Experimental Investigation of Velocity Slip Near an Arcjet Exit Plane," *AIAA Journal*, Vol. 33, No. 2, 1994, pp. 373–375.

[3]Ruyten, W. M., and Keefer, D., "Characterization of Electric Thruster Plumes Using Multiplexed Laser-Induced Fluorescence Measurements," AIAA Paper 92-2965, July 1992.

[4]Ruyten, W. M., Burtner, D., and Keefer, D., "Laser-Induced Fluorescence Measurements on the Plume of a 1 kW Arcjet Operated on Simulated Ammonia," International Electric Propulsion Conf., Seattle, WA, Paper 93-127, Sept. 1993.

[5]Pobst, J. A., Wysong, I. J., and Spores, R. A., "Laser Induced Fluorescence of Ground State Hydrogen Atoms at Nozzle Exit of an Arcjet Thruster," AIAA Paper 95-1973, June 1995.

[6]Cappelli, M. A., and Storm, P. V., "Interior Plasma Diagnostics of Arcjet Thrusters," AIAA Paper 94-2654, June 1994.

[7]Storm, P. V., and Cappelli, M. A., "Laser-Induced Fluorescence Measurements Within an Arcjet Thruster Nozzle," AIAA Paper 95-2381, July 1995.

[8]Butler, G. W., Kashiwa, B. A., and King, D. Q., "Numerical Modeling of Arcjet Performance," AIAA Paper 90-1474, June 1990.

[9]Butler, G. W., Boyd, I. D., and Cappelli, M. A., "Nonequilibrium Flow Phenomena in Low-Power Hydrogen Arcjets," AIAA Paper 95-2819, July 1995.

Shape and Placement of Piezoelectric Sensors for Panel Flutter Limit-Cycle Suppression

Zhihong Lai,* Jen-Kuang Huang,† and Chuh Mei‡
Old Dominion University,
Norfolk, Virginia 23529-0247

Introduction

It is well known that the electrode pattern of piezoelectric materials can be shaped to produce beneficial response of sensors and actuators. Lee and Moon[1] showed that shaped piezoelectric layers can be used as modal sensors and actuators that only sense or actuate certain modes. On the other hand, panel flutter has been encountered in the operation of aircraft and missiles at transonic and supersonic speeds. It is a large-deflection limit-cycle oscillation excited by the airflow[2] that is only on one side of the panel. Lai et al.[3] demonstrated the panel flutter limit-cycle suppression by using piezoelectric actuation with active control. The flutter free region can be enlarged by using the piezoelectric actuation.

In this paper, a method to design sensors (position and rate sensor) for panel flutter suppression is presented. The shape and location of sensors are based on the control feedback gain. The optimal control performance can be achieved by using these sensors with a constant gain direct feedback controller. Numerical simulation is demonstrated for panel flutter suppression by using the shaped sensors designed with this novel approach.

Sensor Design

For curvature sensing, two sensor layers that are placed symmetrically to the midplane are composed as a sensor unit, which is

Received March 2, 1995; revision received June 12, 1995; accepted for publication June 19, 1995.

*Research Associate, Department of Mechanical Engineering.

†Associate Professor, Department of Mechanical Engineering. Senior Member AIAA.

‡Professor, Department of Aerospace Engineering. Associate Fellow AIAA.

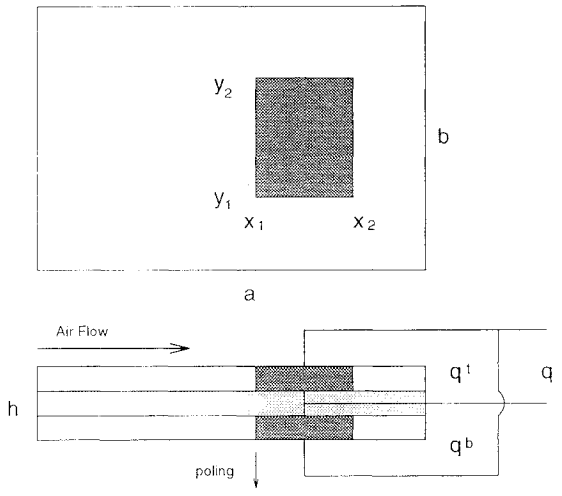

Fig. 1 Configuration of piezoelectric sensor.

shown in Fig. 1. Then, the sensor equation relates the curvature of the panel to the closed-circuit output charge signal[4]

$$q = \int\int_{Se} 2\left\{ -z_k\left[e_{31}\frac{\partial^2 w}{\partial x^2} + e_{32}\frac{\partial^2 w}{\partial y^2} + 2e_{36}\frac{\partial^2 w}{\partial x \partial y}\right]\right\} \mathrm{d}x\,\mathrm{d}y \quad (1)$$

where z_k is the Z coordinate of the midplane of kth piezoelectric layer, e_{ij} is the piezoelectric stress/charge coefficient, and w is the transverse deflection of the panel.

For a simply supported rectangular panel, the flutter deflection of the panel can be expressed as

$$w = \sum_n A_j \sin\left(\frac{j\pi x}{a}\right)\sin\left(\frac{\pi y}{b}\right) \quad (2)$$

By substituting Eq. (2) into Eq. (1), the charge signal for a patched sensor shown in Fig. 1 can be expressed as[4]

$$q = 2hz_k \cos\left(\frac{\pi y}{b}\right)\Bigg|_{y_1}^{y_2} \times \sum_j \left\{ Z_j\left(e_{31}\frac{jb}{a} + e_{32}\frac{a}{jb}\right)\cos\left(\frac{j\pi x}{a}\right)\Bigg|_{x_1}^{x_2}\right\} \quad (3)$$

where $e_{36} = 0$. This equation indicates that the electric charge is a function of the nondimensional modal coordinates $Z_j = A_j/h$ for the given dimensions and location of a sensor.

By taking the time derivative of the Eq. (3), the current signal for the sensor can be expressed as

$$I_s = 2hz_k \cos\left(\frac{\pi y}{b}\right)\Bigg|_{y_1}^{y_2} \times \sum_j \left\{ \dot{Z}_j\left(e_{31}\frac{jb}{a} + e_{32}\frac{a}{jb}\right)\cos\left(\frac{j\pi x}{a}\right)\Bigg|_{x_1}^{x_2}\right\} \quad (4)$$

The innovative concept of the sensor design is to determine the shape and the location of the sensors to achieve the desired control performance with a constant gain direct feedback controller. For the single actuator case, two sensors are generally needed for the feedback controller. One senses the deflection of the panel. Another senses the deflection rate of the panel. The constant gain direct feedback controller is formed by using direct feedback of the charge and the current signal from sensors and is designed to be equivalent with the desired control law. Then, the feedback control law can be expressed as

$$U = -(k_p q + k_d I_s) = -(\boldsymbol{F}_p Z + \boldsymbol{F}_d \dot{Z}) \quad (5)$$

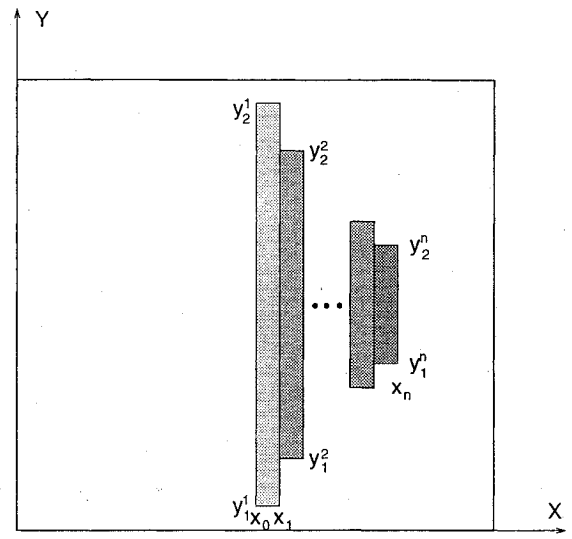

Fig. 2 Layout of piezoelectric sensor stripes.

where k_p and k_d are scalar constants, q is the charge signal that is related to the deflection Z, and I_s is the current signal that is related to the deflection rate $\dot{Z}$. $\boldsymbol{F}_p$ and $\boldsymbol{F}_d$ are desired feedback gain vectors.

First, the sensor for the deflection is considered. The sensor is divided into n (number of system degrees of freedom) stripes. From Eq. (3), the charge signal of ith stripe can be expressed as $q_i = Z_j S_{ji} c_i$, where

$$S_{ji} = -4hz_k\left\{\left(e_{31}\frac{jb}{a} + e_{32}\frac{a}{jb}\right)\cos\left(\frac{j\pi x}{a}\right)\Bigg|_{x_{i-2}}^{x_i}\right\}$$
$$c_i = -\frac{1}{2}\cos\left(\frac{\pi y}{b}\right)\Bigg|_{y_1^i}^{y_2^i} \quad (6)$$

which is a design parameter related to the height of the stripes (see Fig. 2). Since the sensor is placed symmetrically about the centerline of the panel along the x axis, we have

$$y_1^i + y_2^i = b \qquad \text{and} \qquad c_i = -\cos\left(\pi y_2^i/b\right) \quad (7)$$

The charge signal of the sensor is $q = \sum_i q_i = Z^T S C_p$, where $\boldsymbol{C}_p = [c_1\ c_2\ \cdots\ c_n]^T$. Then, from Eq. (5), we have

$$k_p Z^T S C_p = Z^T S \bar{C}_p = F_p Z = Z^T F_p^T \quad (8)$$

where $\bar{C}_p = k_p C_p$. To satisfy the Eq. (8) we have $S\bar{C}_p = F_p^T$. So, if matrix S is full rank, $\bar{C}_p$ can be expressed as $\bar{C}_p = S^{-1}F_p^T$. If all of the elements of $\bar{C}_p$ have the same sign, this means that we can combine all of the stripes into one sensor with one piezoelectric layer. If they do not have the same sign, then the location and width of the stripes need to be adjusted, until all of the elements of $\bar{C}_p$ have the same sign. One has

$$k_p = \max(|\bar{c}_i|) \qquad \text{and} \qquad C_p = (1/k_p)\bar{C}_p \quad (9)$$

For the current sensor, the same logic for the charge sensor design can be applied. One has

$$k_d \dot{Z}^T S C_p = \dot{Z}^T S \bar{C}_d = \dot{Z}^T F_d^T \quad (10)$$

$\bar{C}_d$ can be written as $\bar{C}_d = S^{-1}F_d^T$. If all of the elements of $\bar{C}_d$ have the same sign, then

$$k_d = \max(|\bar{c}_i|) \qquad \text{and} \qquad C_d = (1/k_d)\bar{C}_d \quad (11)$$

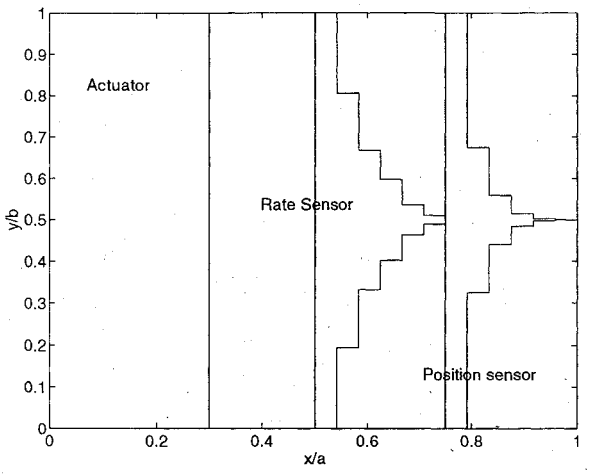

Fig. 3 Shapes and locations of the actuator and position and rate sensors.

The shape of sensor is given by C_d. If all of the elements of $\bar{C}_d$ do not have the same sign, then the location and width of the stripes need to be adjusted, until all of the elements of $\bar{C}_d$ have the same sign.

Simulation and Discussion

Numerical analysis is based on a simply supported square aluminum panel with two piezoelectric laminates that cover the two surfaces of the panel. The physical parameters and the geometry of the panel can be found in Ref. 3. The one-patched actuator is located at the leading edge with the width of 30% panel length. The key for this simulation is to find the location and the shape of the sensor to make all of the elements of vector $\bar{C}_p$ have the same sign. Then, the desired control performance can be achieved through a constant gain direct feedback controller. If the desired control is optimal control, the optimal control performance can be achieved by using the shaped sensors with a constant gain direct feedback controller.

When optimal control is used,[3] the feedback gain varies with the dynamic pressure. Then, the sensor design needs to be updated with the change of the dynamic pressure. It might be interesting to see the constant gain direct feedback control performance by using the shaped sensors designed at the certain dynamic pressure. Here, the dynamic pressure $\lambda = 1500$ is used. Since six modes are used to represent the deflection of the panel in this simulation, the number of sensor stripes should be larger than 12 to get both position and rate sensors. Here, the piezoelectric layer for sensing is divided into 24 stripes. The shape of the position sensor is designed at location $x/a = 0.75$–1. The shape of the rate sensor is designed at location $x/a = 0.5$–0.75. The calculation shows that all of the elements of $\bar{C}_p$ have the same sign with these sensor locations chosen. Then, the location and width of the sensor stripes need not to be adjusted. Figure 3 shows the shapes and locations of the actuator, position, and rate sensors. The position feedback gain k_p is $-449{,}060$, and the rate feedback gain k_d is 0.14954. The maximum suppressible dynamic pressure $\lambda_{\max}$ can reach 1900, which is larger than $\lambda_{\max} = 1744$ obtained by using optimal control.[3] The flutter free region is enlarged about four times of $\lambda_{cr} = 512$. It should be noted that the presented concept can be applied to some other area for the shaped sensor design.

References

[1]Lee, C.-K., and Moon, F. C., "Modal Sensors/Actuators," *Journal of Applied Mechanics*, Vol. 57, 1990, pp. 434–441.

[2]Dowell, E. H., "Nonlinear Oscillations of a Fluttering Plate," *AIAA Journal*, Vol. 4, No. 7, 1966, pp. 1267–1275.

[3]Lai, Z., Xue, D. Y., Huang, J.-K., and Mei, C., "Panel Flutter Limit-Cycle Suppression with Piezoelectric Actuation," *Journal of Intelligent Material Systems and Structures*, Vol. 6, March 1995, pp. 274–282.

[4]Lai, Z., "Vibration Control with Piezoelectric Actuation Applied to Nonlinear Panel Flutter Suppression," Ph.D. Dissertation, Old Dominion Univ., Norfolk, VA, 1994.

Optimal Sensor Location in Active Control of Flexible Structures

Andrzej Maćkiewicz*
Technical University of Poznań, Poznań 60-956, Poland
Jan Holnicki-Szulc†
Polish Academy of Sciences, Warsaw 00-049, Poland
and
Francisco López-Almansa‡
Technical University of Catalonia, 08028 Barcelona, Spain

Introduction

THIS paper presents a new algorithm for the optimal distribution of concentrated sensors to measure displacements or strains in flexible structures; this procedure is applicable in quasistatic shape control (e.g., parabolic mirrors). The proposed approach is based on the analysis of the properties of a linear matrix equation describing the modal strain decomposition, where observable as well as interfering modes are taken into account. To identify n eigenmodes, n sensors are required, and their location should be selected in such a way that the linear system providing the desired n modal amplitudes is well conditioned and the influence of upper modes (observation spillover) is minimized.

Problem Formulation

In this section the problem of static identification of n eigenmodes of deformation when $m + n$ may be relevant is addressed. It can be formulated as the following linear matrix equation:

$$A(\xi)\gamma = b - r(\xi) \tag{1}$$

where the columns of the $n \times n$ matrix A are vectors describing shape functions (at the points where the sensors are located) of the chosen modes; such positions are characterized by the coordinates ξ_i, $\xi^T = (\xi_1, \ldots, \xi_n)$. The vectors γ and b contain the n modal amplitudes to be identified and the n measured quantities, respectively. The vector r represents the perturbation by all the eigenmodes not included in A and is given by

$$r(\xi) = B(\xi)\beta + \rho \tag{2}$$

where the columns of the $n \times m$ matrix B are vectors whose components are the values (at the sensor points) of the m unwanted modes, the m-vector β contains their amplitudes, and the n-vector ρ represents the negligible influence of the residual eigenmodes (other than the $m + n$ ones).

The perturbation vector r changes the solution of the system (1). The optimization problem consists in obtaining ξ so that the relative change $\|\Delta\gamma\|_2/\|\gamma\|_2$ is minimal. Here $\|\cdot\|_2$ is the Euclidean norm ($\|x\|_2^2 := x^T x$). The ratio $\|\Delta\gamma\|_2/\|\gamma\|_2$ can be bounded[1] as follows:

$$\frac{\|\Delta\gamma\|_2}{\|\gamma\|_2} \le \operatorname{cond}[A(\xi)]\,\|r(\xi)\|_2 \frac{1}{\|b\|_2} \tag{3}$$

where $\operatorname{cond}(A) := \|A\|_2\|A^{-1}\|_2$ is the condition number of the matrix A; in this equation $\|\cdot\|_2$ is the matrix norm subordinated

Received May 30, 1995; revision received Dec. 1, 1995; accepted for publication Dec. 5, 1995.

*Professor, Institute of Mathematics, Piotrowa 3a.
†Professor, Institute of Fundamental Technological Research, Świętokrzyska 21.
‡Associate Professor, Architecture Structures Department, Avda. Diagonal 649.